Intrinsic hole localization mechanism in magnetic semiconductors

2004 J. Phys.: Condens. Matter 16 L457

(http://iopscience.iop.org/0953-8984/16/41/L05)

INSTITUTE OF PHYSICS PUBLISHING JOURNAL OF PHYSICS: CONDENSED MATTER

J. Phys.: Condens. Matter **16** (2004) L457–L462 PII: S0953-8984(04)85876-4

LETTER TO THE EDITOR

Intrinsic hole localization mechanism in magnetic semiconductors

H Raebiger[1], **A Ayuela**[1,2] **and R M Nieminen**[1]

[1] Laboratory of Physics, Helsinki University of Technology, 02015 HUT, Finland
[2] Donostia International Physics Center (DIPC), 20018 San Sebastian/Donostia, Spain

Received 3 September 2004
Published 1 October 2004
Online at stacks.iop.org/JPhysCM/16/L457
doi:10.1088/0953-8984/16/41/L05

Abstract

The interplay between clustering and exchange coupling in magnetic semiconductors for the prototype $(Ga_{1-x}, Mn_x)As$ is investigated considering manganese concentrations x of 1/16 and 1/32, which are in the interesting experimental range. For $x \sim 6\%$, we study all possible arrangements of two Mn atoms on the Ga sublattice within a large supercell and find the clustering of Mn atoms at nearest-neighbour Ga sites energetically preferred. As shown by analysis of spin density and projected density of states, this minimum-energy configuration localizes further one hole and reduces the effective charge carrier concentration. Also the exchange coupling constant increases to a value corresponding to lower Mn concentrations with decreasing inter-Mn distance.

Including spin information in semiconductor electronics has enormous potential for new applications (see [1] for a review of magnetoelectronics). Within this field of research, the III–V diluted magnetic semiconductors (DMSs) have opened up a new chapter; in particular, (Ga, Mn)As is a prominent candidate for a spintronics material. This compound, grown by means of low-temperature molecular beam epitaxy (LT-MBE) [2–5], shows ferromagnetism [2–8] with a Curie temperature as large as 110 K in the Mn concentration range between 5% and 10% [3–5]. The ferromagnetism (FM) in (Ga, Mn)As is mediated by holes that are antiferromagnetically (AFM) coupled to the Mn. In spite of the tremendous theoretical effort to explain the interplay of magnetism and semiconductor properties [9–18], a number of fundamental questions still remain unresolved. Such is the so-called hole compensation problem: although the substitutional Mn is a single acceptor and should introduce one hole, the observed hole concentrations are at least an order of magnitude smaller than the Mn concentration [19]. This hole compensation has been ascribed to intrinsic defects such as Mn interstitials [20] and As antisites [12]. However, the antisite concentrations are small, interstitial Mn has a high formation energy compared with substitutional Mn [20, 21], and the interstitial Mn has a rather low migration barrier so annealing will reduce interstitial concentrations [22]. Still, after growth condition optimization and thermal annealing the hole

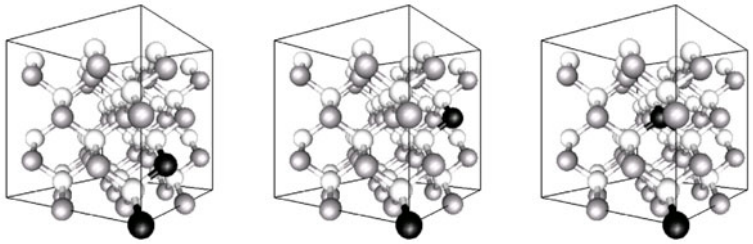

[n-n, ground state (211 meV)] [face, +42 meV (217 meV)] [n-h, +100 meV (160 meV)]

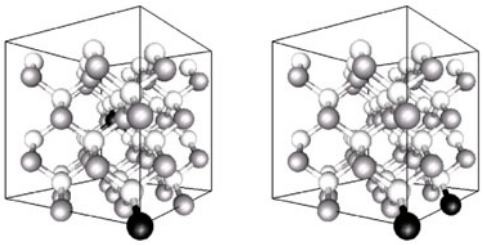

[homog., +114 meV (171 meV)] [edge, +184 meV (67 meV)]

Figure 1. Structures of the $(Ga_{1-x}, Mn_x)As$ system with $x \sim 6\%$ and successive stages of clustering. Ga atoms are shown as grey, Mn atoms as black and As as white. They are ordered according to the energy in millielectronvolts with respect to the ground state, given by the number below the structures. In parenthesis the antiferromagnetic–ferromagnetic AFM–FM energy differences Δ_{AFM-FM} are also provided.

compensation cannot completely be eliminated, and long-time annealing further reduces the hole concentration [8]. We focus on the hypothetical defect-free $(Ga_{1-x}, Mn_x)As$ and consider hole compensation due to intrinsic properties of the substitutional Mn and the spin-polarized holes, bonding and localization effects.

In this letter we present first-principles calculations for magnetic semiconductors. Within the density-functional theory we test all-electron methods, the full-potential linearized augmented plane wave (FLAPW) method [23] and the projector augmented-wave (PAW) method [24, 25], as well as a plane wave pseudopotential (PWPP) method [24]. We also test the generalized gradient approximation (GGA) beyond the local spin density (LSD) approximation [26, 27] for the exchange–correlation functional. We then investigate Mn clustering in (Ga, Mn)As within the supercell approach (see figure 1 describing the considered cases), which gives us hints to comment on hole localization. Based on the clustering results, we re-examine the findings of previous calculations that address the role of the exchange coupling parameter within mean-field theories.

As a benchmark we study zincblende MnAs which is a bulk equivalent to the substitutional Mn in GaAs [9, 13]. To ensure convergence in energy and magnetic moment with respect to k-points and cut-off parameters, the structure of the density of states (DOS) was especially monitored. We see in table 1 obvious differences between our full-potential and pseudopotential calculations for the lattice constants between GGA and LSD results. They show errors of the order of 0.1 Å, which are far from negligible because one is near the transition from metallic behaviour to a half-metallic state. Both the lattice constants and the electronic behaviour show differences with respect to previous calculations [10, 17]. The differences concerning pseudopotential calculations might be ascribed to the pseudopotentials used, while the difference from previous full-potential calculations sounds more puzzling. To correctly observe the metallic or half-metallic behaviour, a denser mesh beyond a typical semiconductor

Table 1. Equilibrium lattice constant and electronic behaviour for the zincblende MnAs structure. The calculations have been done within several density-functional methods with different treatments: (i) for the atom potential (FLAPW and PAW, full potential; PWPP, pseudopotentials); (ii) or for the correlation approximation (GGA, generalized gradient approximation; LSD, local spin density approximation).

	Lattice constant (Å)		Equilibrium behaviour	
	GGA	LSD	GGA	LSD
FLAPW	5.63	5.34	Metallic	Metallic
	—	5.85 [9]	—	Half-metal
PWPP	5.72	5.39	Half-metal	Metallic
	—	5.6–5.7 [13]	—	Metallic
PAW	5.61	5.33	Metallic	Metallic

k-point sampling is required. Apart from the intrinsic pseudopotential differences, the k-point consideration also remains as the main difference with respect to previous pseudopotential calculations (see figure 4 in [17], where the magnetization shows spurious jumps with the distance). The tests clearly show that calculations must be carried out within all-electron methods and the GGA. The PAW calculations are computationally nearly as efficient as the PWPP ones, so the PAW GGA approach is employed henceforth. We have made simulations of $Ga_{1-x}Mn_xAs$ with $x = 1$, $1/16$ and $1/32$ where the notation of x means $\frac{\text{Mn-atoms}}{\text{As-sites}}$ in the supercell. Naturally, the size of the supercell is twice the number of As sites. We only consider substitutional Mn in the Ga sublattice, and focus on the clustering process of two Mn atoms in the high Curie temperature region of $x \sim 6\%$. Here we include two Mn atoms in the 64-atom supercell (i.e. $x = 2/32$) and calculate all five possible Mn arrangements corresponding to different Mn–Mn distances, as shown in figure 1. Again we test for convergence with respect to the number of k-points and cut-off parameters: for the 64 atom supercell a $4 \times 4 \times 4$ mesh including the Γ point is sufficient to sample the Brillouin zone, and plane waves up to the cut-off of 275 eV give converged results. The lattice atoms are relaxed so that the forces in the system are lower than 0.02 eV $Å^{-1}$.

First we investigate the clustering process of Mn on the Ga sublattice. In figure 1 the geometries are ordered according to their energy. The energetic order depends on the Mn–Mn atom distance except for the 'edge' configuration. It is interesting to remark that the nearest neighbour configuration has the lowest energy which indicates clustering, as also predicted using the atomic sphere approximation for the potential [15]. This clustering could play a role in the magnetic order. Thus, the energetic differences $\Delta E_{\text{AFM-FM}}$ between ferromagnetic and antiferromagnetic configurations, i.e. two Mn with parallel or antiparallel magnetic moments, are also given in parenthesis in figure 1. Tests on larger supercells showed that $\Delta E_{\text{AFM-FM}}$ is independent of supercell size. The magnetic ground state of all the configurations is ferromagnetic with a magnetic moment of 4 μ_B/Mn atom in the unit cell, as for the homogenous case in [13]. The $\Delta E_{\text{AFM-FM}}$ values increase when decreasing the Mn–Mn distance. For the edge configuration, the $\Delta E_{\text{AFM-FM}}$ is considerably smaller than in the other configurations. This configuration constitutes an exception because the As atoms are in a more open structure, which enables direct AFM coupling between the two Mn atoms. Considering the other cases, even for the larger distances, in the homogenous distribution, the values $\Delta E_{\text{AFM-FM}}$ are large compared with similar materials [28]. When neglecting the barriers involved in the process, the energies required by the Mn to jump between different Ga sites are smaller than the energies required to flip the spins. In other words, the growth under strong magnetic fields should affect the final atomic configuration.

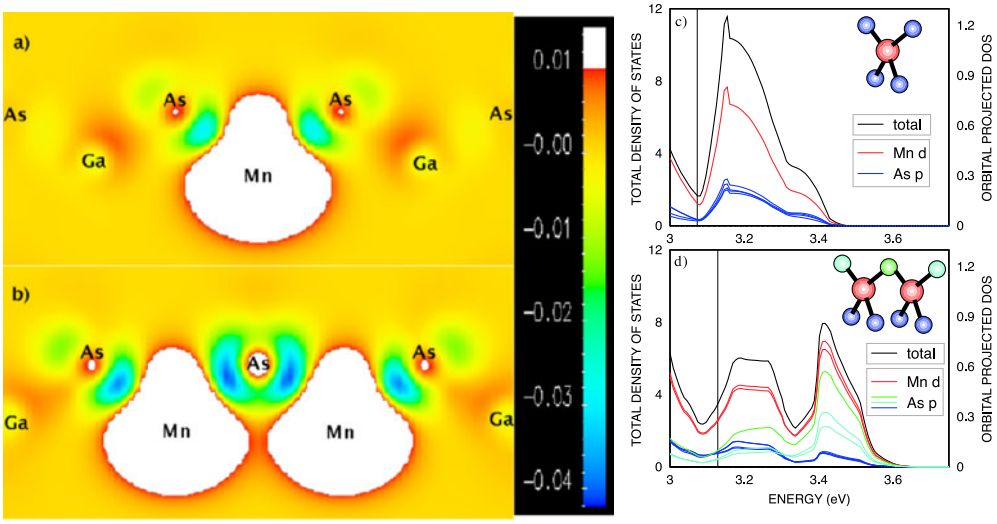

Figure 2. Spin density $\rho_{\uparrow}-\rho_{\downarrow}$ in the (110) plane around Mn ((a) and (b)) and majority spin density of states ((c) and (d)) in the n-n and homogeneous case. Units in μ_B Å^{-3}. Values over 0.1 μ_B Å^{-3} are truncated and given in white. The DOSs are given in states per supercell: the black line for the total DOS and the coloured lines for the orbital projected DOS. The red curve represents Mn d states, the green, turquoise and blue curves represent the As p states corresponding to different As sites, as shown in inset.

Next we focus on the hole localization seen in the spin density as well as the density of states (DOS), and look for quantifications by integrating over both spin density and DOS. The spin polarized charge density for the nearest-neighbour and homogeneous case is presented in figures 2(a) and (b). The negative spin density in the n-n configuration is more concentrated around the As nuclei than in the homogeneous one, especially around the As atom shared as first neighbour by both Mn atoms. As FM is mediated by holes which are AFM coupled to Mn atoms, the negative spin density indicates the hole density. Therefore, this localization of negative spin density implies that the holes undergo strong localization in the n-n case.

This dimmer induced hole localization is further clarified in the DOS shown in figures 2(c) and (d), where the t_d-like hole states split into bonding and antibonding states. Since we are discussing hole states, the behaviour is opposite to electronic states, i.e. the bonding-like hole states are higher in energy (deeper in the gap, larger effective mass and higher localization). From the orbital projected DOS (PDOS) we observe that the As p states around the in-between As (green curve) provide a significant contribution to the DOS in the unoccupied region. In homogeneous case the unoccupied states correspond to antibonding t^a states that account for the Mn induced itinerant hole states responsible for ferromagnetism (see [29]). In the n-n configuration, the t_d symmetry break splits the t^a state into an antibonding state and a bonding-like state deeper in the gap. The deeper state, according to PDOS analysis, is localized around the in-between As, and therefore we are left only with one itinerant t^a-like hole state, reducing the effective carrier concentration by one half.

For a quantitative measure of how the holes are distributed on atomic orbitals we integrate the PDOS over the unoccupied valence band states; the absolute values depend on the basis set used, projection details etc, but relative values provide useful information when comparing different systems. In the dimer configuration we observe 0.1, 0.05 and 0.03 unoccupied p states on the in-between As (green), the end As (turquoise) and the vertical As (blue), respectively following notation in figure 2. In the case of the homogeneous distribution, we observe

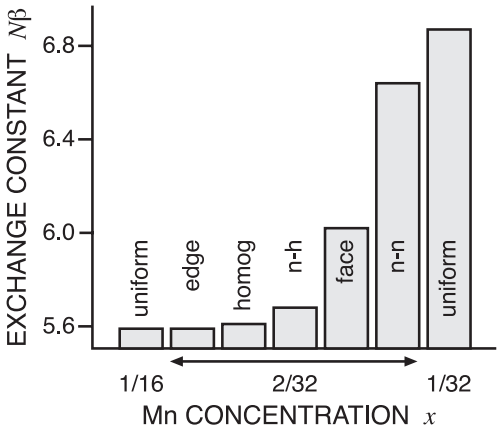

Figure 3. Exchange constant $N\beta$ (in eV) as a function of the Mn concentration x. They are also given as a function of the geometrical arrangement for the Mn concentration $x = 2/32$.

0.04 unoccupied p states on the As next to Mn. It is interesting to compare the integrated hole densities with magnetization around As (i.e. spin density integrated inside a sphere): in the dimer configuration we observe values of -0.077, -0.032 and -0.009 μ_B around the in-between As, end As and vertical As, respectively, while in the homogeneous case the magnetization of the As next to Mn is -0.025 μ_B. The similar values for unoccupied As p states and As magnetization confirm that the negative spin density is actually correlated with the hole density. Notice than both values on the in-between As are over twice those in the homogenous case, which is a non-negligible quantity. Thus this hole localization mechanism seen both in spin density and DOS, combined with the lowered energy in the n-n configuration, is a significant addition to the previously known mechanisms that reduce the effective carrier concentration. With this finding we give a possible explanation why only a fraction of the Mn align ferromagnetically and why a large number of holes is lost, even when we are limited to only Mn in substitutional positions.

The change of DOS and the charge polarization for the different configurations drives us to address the same issues for the exchange coupling parameter $N\beta$, which is crucial in the calculation of thermodynamic properties [18]. Following [13], the effect of the sp–d exchange on the band structure of the host semiconductor can be related to the spin splitting at the gamma point. Although both conduction and valence band splitting can be considered, we concentrate only on the $N\beta$ parameter because it shows the largest changes with the inclusion of magnetism. The valence exchange coupling constant can be written as

$$N\beta = \frac{\Delta E^{v}}{x \cdot \langle S \rangle},$$

where ΔE^{v} is the valence band edge spin splitting at the Γ point, and the mean field spin $\langle S \rangle$ is half of the computed magnetization per Mn ion. Experimentally this constant is extracted from the exciton band that is spin split in optical magnetoabsorption experiments. Our estimated exchange couplings are given in figure 3.

The parameter $N\beta$ for both concentrations shows values between 5.6 and 6.8 eV. With respect to previous PWPP results, 5.48 eV for $x = 1/16$ and 7.34 eV for $x = 1/32$ [13], $N\beta$ does not depend strongly on the Mn concentration. For the concentration $x = 2/32$ the $N\beta$ parameter for several Mn configurations increases as the longest distance between Mn atoms increases. Its value approaches that of the smaller concentration $x = 1/32$. It seems that the longest Mn–Mn distance sets the exchange over the whole semiconductor. A simple mean-field model might after all be justified when re-interpreting the exchange constant in terms of holes ascribed both to Mn and Mn dimers, i.e. the Mn dimer should be treated like

a single Mn impurity. This is because the exchange is mediated by the itinerant holes, and as seen in figure 2(d) in the n-n case the two Mn as a total contribute only one t^a like an itinerant hole. All these findings suggest that the breakdown of the mean-field approximation is not yet well established, i.e. a mean-field scheme may be justified by including this clustering process.

In conclusion, we see that disorder has strong effect on the ferromagnetic coupling. The preferred structural configuration is a dimer of two Mn occupying nearest-neighbour Ga sites. This configuration localizes a hole and explains in part the reduced carrier concentration observed in experiments. Further, our results suggest that the analysis of the breakdown in the mean-field approximation should be reconsidered.

This work has been supported by the Academy of Finland (Centres of Excellence Programme 2000–2005). A Ayuela is supported by the EU TMR programme (contract No ERB4001GT954586). Computer facilities of the Centre for Scientific Computing (CSC) Finland are greatly acknowledged. We thank K Saarinen, K Sato, H Katayama-Yoshida, J von Boehm, M J Puska and M Perez-Jigato for discussions during this work.

References

[1] Prinz G 1998 *Science* **282** 1660
[2] Munekata H, Ohno H, von Molnar S, Segenmüller A, Chang L L and Esaki L 1989 *Phys. Rev. Lett.* **63** 1849
[3] Ohno H 1998 *Science* **281** 951
[4] Ohno H and Matsukura F 2001 *Solid State Commun.* **117** 179
[5] Ohno H 1999 *J. Magn. Magn. Mater.* **200** 110
[6] Ohldag H, Solinus V, Hillebrecht F U, Goedkoop J B, Finazzi M, Matsukura F and Ohno H 2000 *Appl. Phys. Lett.* **76** 2928
[7] Hayashi T, Hashimoto Y, Katsumoto S and Iye Y 2001 *Appl. Phys. Lett.* **78** 1691
[8] Potashnik S J, Ku K C, Chun S H, Berry J J, Samarath N and Schiffer P 2001 *Appl. Phys. Lett.* **79** 3493
[9] Shirai M 2001 *Physica* E **10** 143
[10] Shirai M, Ogawa T, Kitagawa I and Suzuki N 1998 *J. Magn. Magn. Mater.* **177–181** 1383
[11] Ogawa T, Shirai M, Suzuki N and Kitagawa I 1999 *J. Magn. Magn. Mater.* **196/197** 428
[12] Akai H 1998 *Phys. Rev. Lett.* **81** 3002
[13] Sanvito S, Ordejón P and Hill N A 2001 *Phys. Rev.* B **63** 165206
[14] Inoue J, Nonoyama S and Itoh H 2000 *Phys. Rev. Lett.* **85** 4610
[15] van Schilfgaarde M and Mryasov O N 2001 *Phys. Rev.* B **63** 233205
[16] Sanvito S and Hill N A 2001 *Appl. Phys. Lett.* **78** 3493
[17] Sanvito S and Hill N A 2000 *Phys. Rev.* B **62** 15553
[18] König J, Schliemann J, Jungwirth T and MacDonald A H 2003 Ferromagnetism in (II-V) semiconductor *Electronic Structure and Magnetism of Complex Materials* ed D Singh and D A Papaconstatopulos (Berlin: Springer)
[19] Slupinski T, Munekata H and Oiwa A 2002 *Appl. Phys. Lett.* **80** 1592
[20] Erwin S C and Petukhov A G 2002 *Phys. Rev. Lett.* **89** 227201
[21] Mahadevan P and Zunger A 2003 *Phys. Rev.* B **68** 075202
[22] Edmonds K W, Boguslawski P, Yang K Y, Campion R P, Novikov S N, Farley N R S, Gallagher B I, Foxton C T, Sawicki M, Dietl T, Buongiorno Nardelli M and Bernhole J 2004 *Phys. Rev. Lett.* **92** 37201
[23] Blaha P, Schwarz K and Luitz J 1997 *WIEN97* Vienna University of Technology
An improved and updated Unix version of the copyrighted WIEN-code, was published by Blaha P, Schwarz K, Sorantin P and Trickey S B 1990 *Comput. Phys. Commun.* **59** 399
[24] Kresse G and Furthmüller J 1996 *Phys. Rev.* B **54** 11169
Kresse G and Furthmüller J 1999 *VASP the Guide* (Vienna: Vienna University of Technology) http://tph.tuwien.ac.at/~vasp/guide/vasp.html
[25] Kresse G and Joubert D 1990 *Phys. Rev.* B **41** 5414
[26] Perdew J P, Vosko J A, Vosko S H, Jackson K A, Pederson M R, Singh D J and Fiolhais C 1992 *Phys. Rev.* B **46** 6671
[27] Perdew J P and Wang Y 1992 *Phys. Rev.* B **45** 13244 and references therein
[28] Sanyal B, Bengone O and Mirbt S 2003 *Phys. Rev.* B **68** 205210
[29] Sato K, Dederichs P H and Katayama-Yoshida H 2003 *Europhys. Lett.* **61** 403